ChemPubSoc Europe

DOI: 10.1002/chem.201902975

CHEMISTRY A European Journal Full Paper

Liquid Crystals | *Hot Paper*

Synthesis, Thermal, and Optical Properties of Tris(5-aryl-1,3,4-oxadiazol-2-yl)-1,3,5-triazines, New Star-Shaped Fluorescent Discotic Liquid Crystals

Natalie Tober,[a] Thorsten Rieth,[a] Matthias Lehmann,*[b] and Heiner Detert*[a]

Dedicated to Professor Herbert Meier, Mainz, on the occasion of his 80th birthday

Abstract: The synthesis of tris(aryloxadiazolyl)triazines (TOTs), C_3-symmetrical star-shaped mesogenes with a 1,3,5-triazine center, 5-phenyl-1,3,4-oxadiazole arms, and various peripheral alkoxy side chains is reported. Threefold Huisgen reaction on a central triazine tricarboxylic acid and suitable aryltetrazoles yields the title compounds. Selected analogues with a benzene center are included in this study and allow for an evaluation of the impact of the central unit on the physical properties. Thermal (differential scanning calorimetry, DSC; polarization optical microscopy, POM), optical (UV/Vis, fluorescence), electric (time of flight, TOF), and structural (single crystal; wide-angle X-ray scattering, WAXS) properties of these compounds were investigated. The modification of alkoxy chain length and substitution pattern allows for a tuning of the physical properties. TOTs emit blue to yellow light, depending on conjugation length, donor–acceptor substitution, and solvent polarity, whereas concentration quenches and aggregation enhances the emission. The width of the mesophases is typically around $\Delta T = 100$–150 K but can even exceed 220 K. Polarization optical microscopy and X-ray diffraction on oriented filaments reveal that TOTs are highly ordered liquid crystals (LCs) with long-range hexagonal columnar structure.

Introduction

The development of new materials for electronic and optoelectronic devices, for example nonlinear optical (NLO) absorbers, emitters, and semiconductors for the application in solar cells, light-emitting diodes (LEDs), field-effect transistors (FETs), and quantum computers is a highly active research field with an extraordinary commercial potential.[1–4]

Especially organic compounds are of great interest, they are required to replace rare, toxic, and expensive inorganic materials.[3,5] Organic optoelectronic devices have already been developed, like organic photovoltaics (OVPs),[6] organic light-emitting diodes (OLEDs),[7] and organic field-effect transistors (OFETs).[8] Although calamitic liquid crystals are the key compound in LCDs,[2,8,9] the technology of discotic liquid crystals (DLC) is only in its beginning.[10,11] Further interesting features of DLCs are self-assembly, mostly to form columnar mesophases, self-healing, and aggregation-induced emission enhancement.[12] The columnar arrangement enables a one-dimensional charge transfer (CT)[4,10] by overlapping of the aromatic π-orbitals (π-stacking).[13] Most DLCs consist of an electron-rich aromatic core, for example triphenylene, (triaza)truxene, or thiophene, often with electron-rich arms like alkoxybenzene or thiophene.[9,14,15] In contrast, electron-deficient heterocycles like pyrimidines, triazines, or oxadiazoles are less common as components of the π-conjugated core.[13,16–18]

1,3,5-Tris-(5-phenyl-1,3,4-oxadiazol-2-yl)benzene (TOB), one of the first reported discotic oxadiazole compounds,[19] melts at 335 °C without any liquid-crystalline phase, but a few molecules of this structure with flexible side chains attached are reported to form broad mesophases with the characteristic textures of a columnar arrangement, as observed by polarization optical microscopy.[20,21]

The substitution of benzene with 1,3,5-triazine leads to a new core for discotic liquid crystals: tris(aryloxadiazolyl)triazine (TOT, **N1**–**N15**, Scheme 1, Figure 1), a fluorescent scaffold with excellent tendency towards columnar arrangement in the LC phase and broad mesophases. The synthesis as well as the thermal, optical, and luminescent properties of these compounds and some benzene analogues (TOBs **C2**–**C11**) and the comparison of their properties are subject of this report.

[a] *N. Tober, Dr. T. Rieth, Prof. Dr. H. Detert*
Institute of Organic Chemistry, University of Mainz
Duesbergweg 10–14, 55128 Mainz (Germany)
E-mail: detert@uni-mainz.de

[b] *Prof. Dr. M. Lehmann*
Institute of Organic Chemistry, University of Würzburg
Am Hubland, 97074 Würzburg (Germany)
E-mail: matthias.lehmann@uni-wuerzburg.de

Supporting information and the ORCID identification number(s) for the author(s) of this article can be found under: https://doi.org/10.1002/chem.201902975.

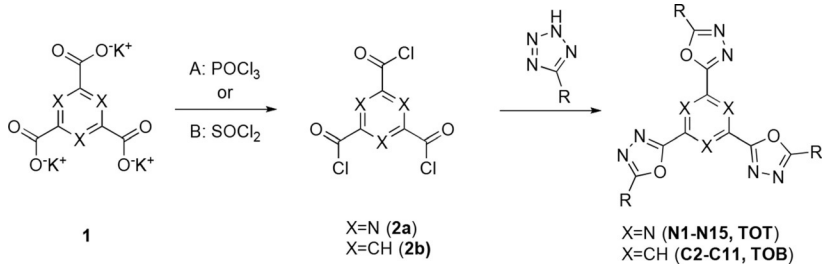

Scheme 1. Huisgen reaction (yields: 13–72%).

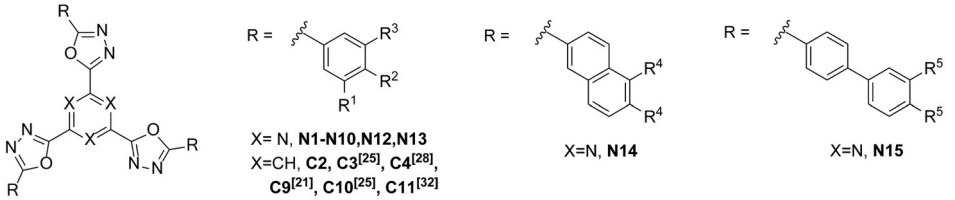

Figure 1. Synthesized compounds and analogues from literature.

Results and Discussion

Synthesis

The common route to 1,3,4-oxadiazoles is the stepwise formation of diacylhydrazine followed by dehydration/cyclization with $POCl_3$.[21–23] This method has been successfully applied for the synthesis of star-shaped molecules with a benzene center. An alternative way to construct oxadiazoles is opened by the Huisgen reaction of tetrazoles and acid chlorides in presence of pyridine bases.[20,24,25] This method is particularly rewarding for the preparation of sensitive products.[26] Hence, we followed this strategy to build discotic LCs with a tris-1,3,4-oxadiazolyl-1,3,5-triazine nucleus **N1**–**N15** (Scheme 1).

Initial results were disappointing because upon addition of tris(chlorocarbonyl)triazine **2a** to the tetrazole/collidine mixture, a brown precipitate was formed and tetrazoles were converted to nitriles (determined by mass spectrometry). Given that the acid chloride **2a** decomposed in the presence of bases and that no oxadiazole was formed, the reaction had to be performed in the absence of bases regardless of some side reactions due to HCl. Good yields of heterocyclic stars **N1**–**N15** were obtained, accompanied by small amounts of 1,2,4-triazoles as byproducts (determined by NMR, MS).

The required triazine acid chloride **2a** was prepared in three steps by acid-catalyzed trimerization of ethyl cyanoformate, saponification, and chlorination of the tripotassium salt **1** with $POCl_3$ to obtain pure **2a** in 71% yield after distillation (method A). Similar results in the Huisgen reaction were obtained when **1** was converted to **2a** with thionyl chloride and the excess chlorinating agent was evaporated (method B).[28] It appeared to be essential that **2a** was prepared just before the Huisgen reaction.

The tetrazoles were synthesized in multistep reactions starting with protocatechuic nitrile **3** or methyl gallate **6** (Scheme 2).[29,30] 3,4-(Dialkoxyphenyl)-tetrazoles **5a**,**b** are accessible through alkylation of **3** and 1,3-dipolar cycloaddition of an azide.[29] The 3,4,5-analogues **9a**–**c** were synthesized from methyl gallate **6** through alkylation, saponification, chlorination/ammonolysis followed by dehydration/ azide transfer with

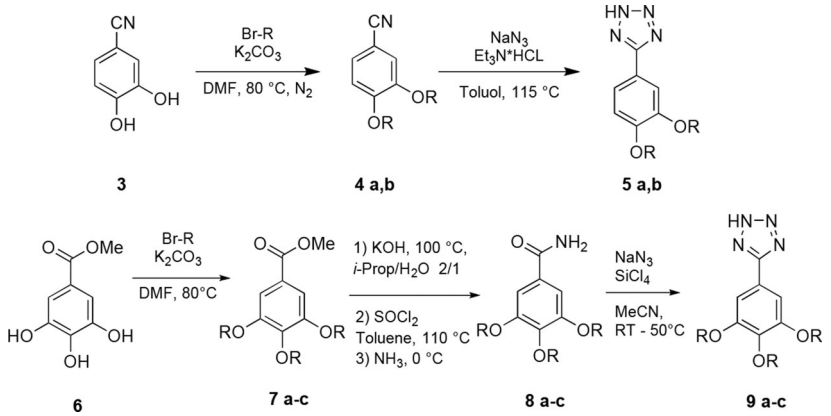

Scheme 2. Synthesis of tetrazoles.

triazidichlorosilane (see the Supporting Information for details).[31]

Biphenyl tetrazole **10** is accessible through Suzuki cross-coupling reaction of iodophenyl tetrazole and di(decyloxy)phenyl boronic acid.[32] 5,6-Di(decyloxy)naphth-2-yl-tetrazole **11** was prepared by oxidation of 6-bromo-2-naphthol to the *o*-quinone, reduction, alkylation and Rosenmund-von-Braun cyanation followed by azide addition, similar to a literature procedure.

With these tetrazoles in hand, 14 different tris(aryloxadiazolyl)triazines (TOT, **N1**–**N15**) and four tris(oxadiazolyl)benzenes (TOB, **C2**–**C4, C9**) were synthesized in yields ranging from 13–72% (Figure 1, Table 1). Triazoles were formed as byproducts, their chromatographic behavior is generally very similar to the tris(oxadiazolyl) stars. Therefore, excessive chromatography was occasionally required—and responsible for reduced yields. Residual triazole in the yellow fluorescent TOT is easily distinguished by its blue fluorescence on solvent-loaded TLC plates. The identity and purity of all materials is demonstrated by standard analytical methods, such as ^{1}H and ^{13}C NMR as well as TLC and HR-MS.

For the synthesis of the carbon analogues **C2**–**C9**, the reaction of trimesic acid trichloride **2b** in the presence of 2,4,6-collidine successfully gave the pure TOBs in yields up to 61% after chromatography.

Thermal properties: DSC and POM

Polarized optical microscopy revealed birefringend mesophases for 18 out of 20 star-shaped molecules (including 2 mesogenes from literature).[23,27] The LC-phases show textures typical for hexagonal-columnar arrangements (Figure 2a,b). A standard discotic liquid crystal exhibits usually two transitions in a DSC heating scan, melting and clearing. TOTs and TOBs are highly viscous liquid crystals in the high-temperature range as evidenced by shearing experiments. Upon cooling, the structure and texture of the mesophase is maintained, even after complete congealing. Therefore, determination of the melting point is hard to observe by POM. In highly viscous mesophases (TOTs and TOBs), crystallization can be slow, resulting in partial or complete preservation of the mesophase structure. As a consequence, measured melting enthalpies in the cooling scan

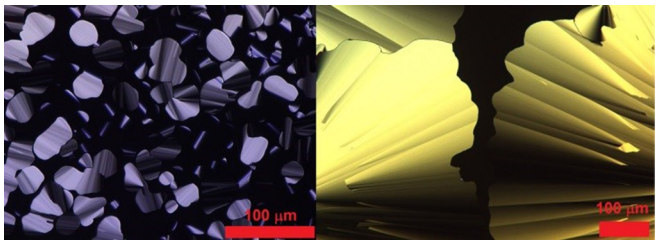

Figure 2. a) POM: fan texture of (**N8**) at 200 °C (0.5 K min^{-1}) upon cooling. b) POM: focal conic fan texture of (**N2**) at 195 °C (10 K min^{-1}) upon cooling.

are lower than those of the first heating cycle. Thus, the values in Table 2 are for not completely relaxed materials. These phenomena have been observed for several TOTs and TOBs (**N2**–**N8**, **N14**, **C2**, **C3**). The partial recrystallization can give rise to a cold crystallization just below the melting point during the subsequent heating scan (**N5**, **N7**, **N14**). Glass transitions were detected for **N12** and also transitions between crystal phases (**N15**, **C3**, **C9**) which occur only in the first heating curve or after prolonged storage.

TOTs **N6** and **N8** are strongly inhibited in crystallization, a second measurement of the same DSC sample after two months did not exhibit any Cr→M transitions, only after two years a DSC experiment revealed a signal attributed to such a transition. Furthermore, some TOTs show exothermic transitions in their second heating cycles (e.g., **N5**, Figure 3) caused by thermally induced crystallization.[33] This is followed by two endothermic transitions, melting ($T = 88.5$ °C, $\Delta H = 46.0$ kJ mol^{-1}) and clearing ($T = 184.3$ °C, $\Delta H = 3.9$ kJ mol^{-1}).

The results of POM and DSC investigations on TOTs and TOBs are summarized in Figure 4 and Table 2. TOTs and TOBs show broad mesophases with phase widths of 69–220 K. Generally, the triazine-based compounds have lower melting and higher clearing temperatures than their carbon analogues and consequently, the mesophase ranges are 20–64 K wider (Figure 4). The transition temperatures of 3,4-dialkoxy TOTs **N2**–**N5** are weakly affected by elongation of alkyl chains (octyl–tetradecyl); the maximal T_c is reached with decyl and dodecyl chains. T_c is more influenced by chain length than T_m. The sensitivity of transition points to chain length is more pronounced in the 3,4,5-trialkoxy series **N8**–**N10**. Compared with

Table 1. Tris(aryl-1,3,4-oxadiazolyl)triazines and -benzenes, substitution pattern, chain length, yield (over two steps), and references.

	R	Yield [%]		R	Yield [%]
N1	$R^1 = R^3 = H$, $R^2 = n$-propyloxy	47[a]	**N8**	$R^1 = R^2 = R^3 = n$-hexyloxy	31[b]
N2	$R^1 = H$, $R^2 = R^3 = n$-octyloxy	48[a]	**N9**	$R^1 = R^2 = R^3 = n$-octyloxy	34[a]
C2	$R^1 = H$, $R^2 = R^3 = n$-octyloxy	61	**C9**	$R^1 = R^2 = R^3 = n$-octyloxy	13; 28[21]
N3	$R^1 = H$, $R^2 = R^3 = n$-decyloxy	38[a]	**N10**	$R^1 = R^2 = R^3 = n$-decyloxy	45[a]
C3	$R^1 = H$, $R^2 = R^3 = n$-decyloxy	59[c][23]	**C10**	$R^1 = R^2 = R^3 = n$-decyloxy	–[c][23]
N4	$R^1 = H$, $R^2 = R^3 = n$-dodecyloxy	47[a]	**C11**	$R^1 = R^2 = R^3 = n$-dodecyloxy	–[c][27]
C4	$R^1 = H$, $R^2 = R^3 = n$-dodecyloxy	33; 87[25]	**N12**	$R^1 = R^2 = R^3 = 2$-ethylhexyloxy	55[b]
N5	$R^1 = H$, $R^2 = R^3 = n$-tetradecyloxy	70[b]	**N13**	$R^1 = R^2 = R^3 = 3,7$-dimethyloctyloxy	72[b]
N6	$R^1 = H$, $R^2 = R^3 = 4$-ethyloctyloxy	52[b]	**N14**	$R^4 = n$-decyloxy	46[b]
N7	$R^1 = H$, $R^2 = R^3 = 3,7$-dimethyloctyloxy	29[b]	**N15**	$R^5 = n$-decyloxy	49[b]

[a] Method A: $C_3N_3(COOK)_3$, $POCl_3$. [b] Method B: $C_3N_3(COOK)_3$, $SOCl_2$. [c] Trimesic acid chloride.

Table 2. Phase-transition temperatures (°C) and corresponding enthalpies [kJ mol^{-1}].

Compound		Compound	
N1	Cr 276 I	**N8**	Cr 55 [24.8][c] M 220 [1.2][c] I
N2	Cr 97 [3.7][b] Col_h 192 [3.4][b] I	**N9**	Cr −10 [Tg][b] Col_h 210 [4.5][b] I
C2	Cr 106 [67.1] Col_h 181 [4,8] I	**C9**	Cr 1 [8.0] Cr 34 [20.9] Col_h 190 [4.9] I
N3	Cr 84 [3.9][b] M 203 [4.3][b] I	**N10**	Cr 33 [21.9][a] M 179 [4.0][b] I
C3[23]	Cr 51 [92.7] Cr 83 [189.6] Cr 107 [26.7] M 176 [18.4] I	**C10**[23]	Cr 46 [86.2] M 169 [15.5] I
N4	Cr 87 [3.4][b] M [4.9][b] 202 I	**C11**[27]	Cr approx. 20 M approx.145 I
C4[25]	Cr 103 [54.4] M 184 [3.9] I	**N12**	I
N5	Cr 89 [46.0][b] M 184 [3.9][b] I	**N13**	Cr −19 [Tg][c] M 72 [0.9][b] I
N6	Cr 56 [2.9][c] M 156 [2.3][c] I	**N14**	Cr 121 [1.9][b] M 210 [3.0][b] I
N7	Cr 95 [0.6][a] M 170 [2.1][b] I	**N15**	Cr 93 [4.1][b] Cr 165 [26.9][b] I

[a] Onset of the signal in first heating cycle. [b] Onset of the signal in second heating cycle. [c] Onset of the signal in heating cycle of the second measurement. Cr: crystalline; Col_h: columnar hexagonal; M: mesomorphic; I: isotropic.

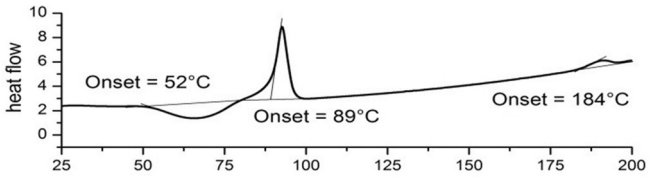

Figure 3. DSC: second heating curve of (**N5**).

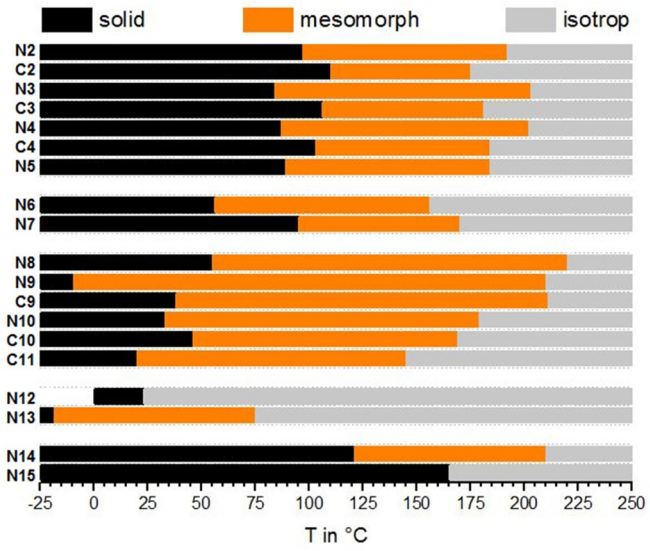

Figure 4. Overview of phase width of tris(aryloxadiazolyl)arene stars.

the 3,4-dialkoxy derivatives, their LC phases are much wider (up to 220 K!) and appear at significantly lower temperatures.

Branching in the alkyl chains of the triazine stars (**N6**, **N7**, **N12**, **N13**) reduces transition temperatures and width of the LC phase. This effect is more pronounced in the 3,4,5-trialkoxy series, even a complete loss of mesomorphism has been found (**N12**). This can be due to two reasons: diastereomeric mixtures and steric crowding, especially for the 3,4,5-trialkoxy series.

Extending the aromatic system of TOTs from peripheral phenyl (**N3**) to peripheral naphthalene **N14** results in an increase of the melting point by 37 K and of the clearing point by 7 K. The even longer biphenyl derivative **N15** reveals only a crystalline phase at much lower temperature, which may be attributed to the nonplanar structure of this building block and therefore reduced mobility in a column. The thermal behavior (Cr 25 (6) Col_h 114 (4) iso) of a thiophene analogue to **N9** and a higher homologue reveals a strong stabilization of the mesophase by the oxadiazole, probably due to CT interactions between electron-deficient oxadiazoles and alkoxyphenyl rings.[34] Similarly, 1,2,3-triazoles stabilize the mesophase, phase widths are in the range of 160 K.[17]

X-ray scattering

Single crystals of *p*-propyloxy-TOT **N1** were obtained through slow evaporation of toluene solution of **N1**.[35] Compound **N1** crystallizes in the triclinic space group $P\bar{1}$ ($a=8.62$, $b=13.59$, $c=15.79$ Å; $\alpha=89.91$, $\beta=85.75$, $\gamma=76.78°$) and contains two molecules per unit cell (Figure 5). Crystallographic data exhibit a nonplanar molecular structure. In contrast to the expected C_3-symmetry (Figure 5), **N1** adopts a Y-shape because one phenyloxadiazole arm is flipped around the triazine–oxadiazole bond. These rings show a dihedral angle of 16° whereas all other biaryl units are essentially planar ($\Theta \leq 1°$). The dihedral angles between the benzenes and oxadiazoles are about 10–14°. Furthermore, two propyloxy unit are disordered.

The broken symmetry has also been observed for a tris-1,2,3-triazolyl-1,3,5-triazine,[36] but a star similar to **N1** with thiophene instead of oxadiazole[34,37,38] shows nearly perfect C_3-symmetry. This was explained by attractive S–N interactions. The high planarity, as expressed by dihedral angles between the heterocycles of 1–11°, was found to improve charge-transport properties. Although these molecules are rotationally displaced with respect to adjacent molecules, the packing of Y-shaped **N1** corresponds to columns of alternating oriented molecules along a diagonal through the unit cell. Each two molecules have a center of inversion and the central triazines are off-diagonal, bringing oxadiazoles and alkoxyphenyl in close proximity. These features correspond to the results of simulation of the mesophase structure (see below).

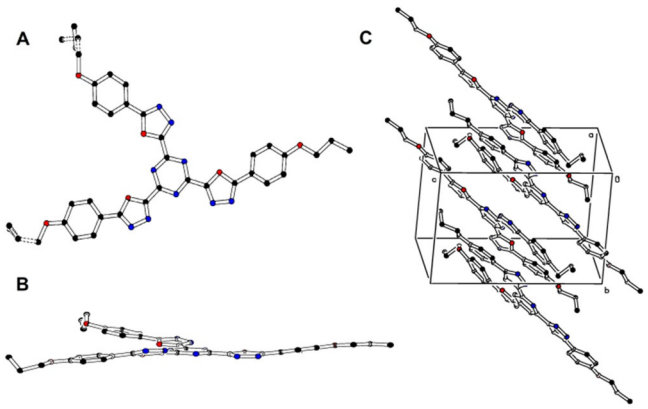

Figure 5. Single-crystal structure of **N1** A) asymmetric molecular Y-conformation, B) nearly perfect planarity, C) unit cell with alternating arranged molecules.

2D-Scattering on oriented fibers

Two-dimensional wide-angle X-ray scattering (WAXS) experiments on macroscopically aligned extruded fibers were carried out to determine the intra- and intercolumnar organization of the TOTs and TOBs in their liquid-crystal phases.

Filaments were obtained by extrusion of **N2** and **N9** in their LC-phase (175 °C, 10 min annealing) as well as of **C2** and **C9** (140 °C, 5 min annealing). Table 3 and Figure 6 summarize the results. The patterns in Figure 6A,B reveal characteristic features of well-aligned columnar LC samples: i) reflections centered at the equator attributed to a hexagonal 2D lattice of columns, ii) a halo corresponding to the liquid-like chains with an average distance between 4.0–4.6 Å (see Table 3) and iii) a rather broad signal at wider angles reminiscent of the average aromatic distances (π–π stacking). The corresponding integration of the patterns along the equator and the meridian (Figure 6C,D) uncover general trends. First, the reflections with larger and mixed indices are obviously more intense for the carbon derivatives than for the nitrogen derivatives. For **N2** the 11 and 20 reflections appear only at lower temperature.

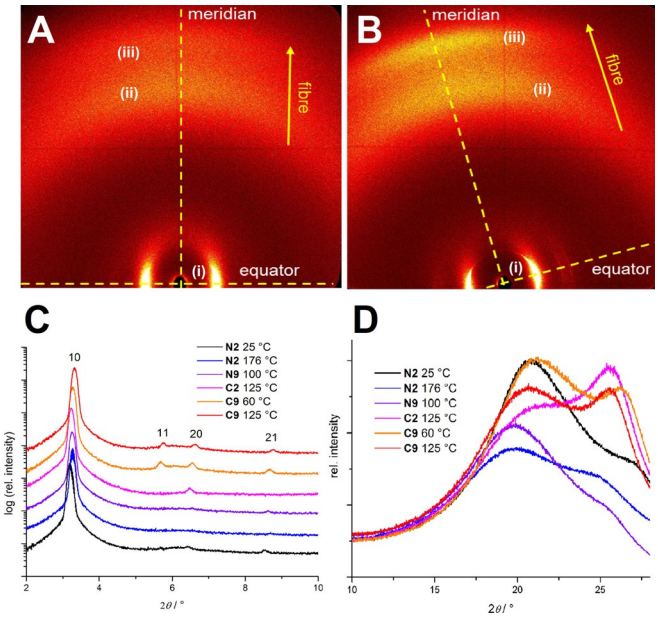

Figure 6. Diffraction pattern of **N2** at 176 °C (A) and **C9** at 125 °C (B). (C) and (D) show the integrated intensity of the equator and the meridian at various temperatures.

This points to a higher two-dimensional order of columns for the derivatives **C2** and **C9** when compared with **N2** and **N9**. The cell parameters of the hexagonal unit cells decrease with increasing temperature (see also Table 3), whereas simultaneously the distances along the columns increase. However, this effect is surprisingly small because *a* changes only by 0.7 Å, when heating **N2** from 25 to 176 °C. These observations are the same for the nitrogen and the carbon series. The distinct difference in both series is the intensity of the π–π signal corresponding to distances between 3.2–3.5 Å, which is much more intense for the compounds **C2** and **C9** and very small or almost absent for **N2** and **N9**. The correlation length calculated by the Scherrer formula[39] amounts to 6–7 repeating units for **C2**, **C9** and only about 4 repeating units for **N2** and **N9**. To gain insight in the packing of these star-shaped, shape persistent mesogens, the density was measured at 23.5 °C and extrapolated to the temperatures of the LC phases (Table 4, for details see the Supporting Information).

Table 3. Unit cell parameters, miller indices and corresponding distances.

Compound	hkl (*d* in Å)						
N2	100		200	210	halo	π–π	a_{hex} = 30.8 Å
176 °C	(26.7)		(13.3)	(10.1)	(4.6)	(3.5)	
N2	100		200	210	halo	π–π	a_{hex} = 31.5 Å
25 °C	(27.3)		(13.7)	(10.3)	(4.2)	(3.2)	
C2	100		200		halo	π–π	a_{hex} = 31.5 Å
125 °C	(27.3)		(13.6)		(4.0)	(3.5)	
N9	100		200	210	halo	π–π	a_{hex} = 31.2 Å
100 °C	(27.1)		(13.6)	(10.2)	(4.5)	(3.5)	
N9	100		200	210	halo	π–π	a_{hex} = 31.5 Å
25 °C	(27.3)		(13.7)	(10.3)	(4.3)	(3.3)	
C9	100	110	200	210	halo	π–π	a_{hex} = 30.7 Å
155 °C	(26.6)	(15.3)	(13.4)	(10.1)	(4.3)	(3.5)	
C9	100	110	200	210	halo	π–π	a_{hex} = 30.8 Å
125 °C	(26.7)	(15.4)	(13.3)	(10.1)	(4.1)	(3.4)	
C9	100	110	200	210	halo	π–π	a_{hex} = 31.3 Å
60 °C	(27.1)	(15.6)	(13.5)	(10.2)	(4.0)	(3.4)	

Table 4. Experimental, extrapolated densities, and number of molecules in a columnar repeating unit *h*.

	ρ_{exp}[a] [g cm^{-3}]	V_{mol}[b] [Å^3]	V_{Ar}[c] [Å^3]	V_{IAr}[d] (crystal) [Å^3]	ρ[e] [g cm^{-3}] (T [°C])	Z[f]	h[g] [Å]
N2	1.065	2000	698	609	1.02 (100)	3	7.50
N9	1.012	2736	783	625	0.96 (100)	2	6.84
C2	1.029	2065	763	616	0.97 (125)	3	7.68
C9	1.022	2704	751	632	0.95 (125)	2	7.08

[a] Experimental density at 23.5 °C (buoyancy method). [b] Molecular volume at 23.5 °C. [c] Aromatic volume at 23.5 °C. [d] Incremental aromatic volume. [e] Estimated densities at different temperatures (calculation see the Supporting Information). [f] Number of molecules *Z* in the columnar repeat. [g] Columnar repeat.

From the density data, the molecular volume was calculated and subsequently the aromatic volumes are available when the known volumes of the aliphatic chains are subtracted.[40] Here it is evident that all aromatic volumes are larger than the volumes occupied in a crystal, which were calculated by an increment method.[41] The volumes are 15–25% higher in the mesophases. This is certainly a consequence of the less dense packing in the soft-crystalline and liquid-crystalline matter but the large values points also to the fact that the intrinsic free space between the shape-persistent branches cannot be completely filled. There is clearly much less free space in the aromatic part for the derivative **N2** with six chains, which has the highest density. The integer number of molecules filling the columnar repeating *h* unit (twice the π–π distance) was calculated to be three molecules for the six-chains derivatives and two molecules for the columnar stratum of the nine-chain mesogens. For all systems, the number of aliphatic chains is identical, the *a*-parameter is also almost identical and, therefore, the value *h* must increase for **N2** and **C2** owing to the larger number of aromatic units in the core area of the column. However, this increase amounts only to 0.6–0.7 Å and assuming coplanar stacked mesogens **N2** and **C2** would be only 2.5–2.6 Å apart, whereas the intramolecular distances for **N9** and **C9** are in agreement with π-stacks (3.4–3.5 Å). Given that the distances between the six-chain derivatives are smaller than van der Waals distances, modelling of the LC phases has been performed to unravel packing details. Thus, the columnar phases of **N2**, **N9**, and **C9** were constructed with the program Materials Studio (Forcite, COMPASS II) on the bases of XRS and density data. Figure 7 highlights the results for compound **N2**. Various starting setups with non-C_3-symmetric and C_3-symmetric conformers were geometry optimized to obtain large attractive noncovalent interaction energies after several minimization and annealing procedures. In general, the van der Waals energy was large and negative (−1670 to −1768 kcal mol^{-1}, values are given for a set of four unit cells with 24 molecules), whereas the electrostatic energy was always positive but decreased slightly when compared with the single molecule (850–898 kcal mol^{-1} in the LC phases versus 973 kcal mol^{-1} for the single molecule, see the Supporting Information).

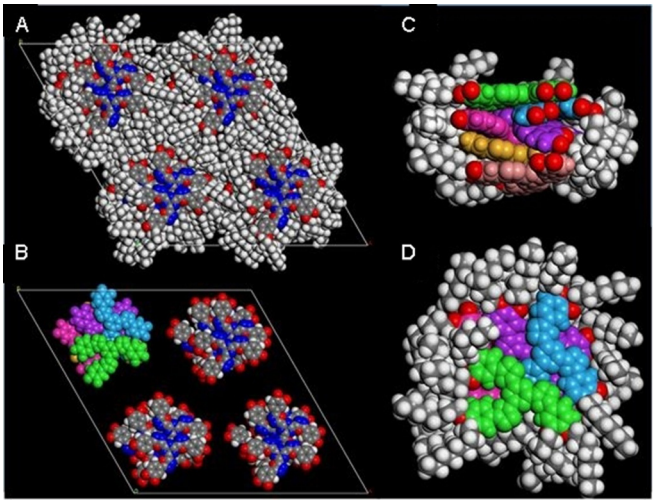

Figure 7. Packing of **N2** in the columnar assembly. Molecules are displaced from the center of the column and occupy spaces from different columnar slices to fill efficiently the space.

The best results were obtained for the Y-shaped conformer similar to the one found in the single crystal. It was observed that the core position deviates from the center of the column (Figure 7C) and that the aromatic units contribute to the space filling of different columnar slices (Figure 7D). The chains densely occupy the peripheral space. As a consequence of this dense packing, the intracolumnar order is reduced and almost no π-stacking is visible in the experimental pattern. However, note that **C2**, with the same number of mesogens per columnar stratum, must pack in as similar way but nevertheless, exhibit a π-stacking signal. Consequently, the electrostatic repulsion discussed in detail below must also be important for the LC self-assembly. When comparing **N9** and **C9**, it was evident that the columnar stratum of height *h* consists of two molecules with 18 chains and the intracolumnar spacing was calculated to be 3.4 (**N9**) and 3.5 Å (**C9**). This can be also confirmed by modelling (see the Supporting Information). Although **C9** shows a clear π-stacking of the mesogens, **N9** lacks this signal. The missing π-stacking for **N9** may be explained by the increase in the electrostatic interactions for **N9** compared with single molecules, whereas the electrostatic interactions do not change for **C9** (see the Supporting Information).[42] Thus, mesogens **N9** avoid evidently the cofacial stacking.

Electrical conductivity of N2, C2 and N9

Conductivity was studied using the Time-of-Flight method to get information about their charge-transfer ability (see the Supporting Information). For the 3,4-substituted derivative **N2**, charge carrier mobilities of $\mu = 10^{-3}$ cm^{2}V^{-1}s^{-1} in the crystalline (25 °C) and mesophase (120 °C) are significantly higher than those of its carbon analogue **C2** and the 3,4,5-substituted **N9**, which are in the range of $\mu = 10^{-5}$ cm^{2}V^{-1}s^{-1} at 120 °C. The latter can be rationalized by the much denser packing of the aromatic scaffold in the center of the columns when considering **N2** and **N9**. The lower charge-carrier mobility of **C2** is not yet well understood, because the aromatic units pack as compact as **N2**, and moreover, show a clear signal for a higher intracolumnar order in contrast to **N2**.

Optical spectroscopy

Solid tris(oxadiazolyl)triazines are yellow (branched alkoxy chains) to red (3,4,5-*n*-alkoxy substituted TOTs) compounds whereas the TOBs are colorless. In solution, the latter absorb only in the UV range ($\lambda_{max} \approx 325$ nm, $\lambda_{0.1} \approx 360$ nm) whereas the absorption bands of TOTs extend into the blue region ($\lambda_{max} =$ 360–400 nm, $\lambda_{0.1} \approx 406$–478 nm. A comparison with analogous stars with thiophene[34,37] or 1,2,3-triazole[17,18] replacing the oxadiazole in TOTs reveals a similarity between oxadiazole and thiophene stars, the latter absorb at slightly longer wavelengths ($\Delta\lambda \approx 8$ nm). In contrast, the UV spectra of 1,2,3-triazole derivatives peak about $\Delta\lambda \approx -75$ nm at shorter wavelengths.[34]

The excitation maxima of triazine-centered stars (**N1**, **N2**, **N9**, **N14**) in cyclohexane are nearly independent from the analytes' polarity and peak between 380 and 385 nm. Only the absorption maximum of biphenyl **N15** is at higher energy (λ_{max} = 365 nm). Change of solvent has nearly no effect on the absorption spectra, except **N14**, **N15** with the extended π-systems; here, solvatochromic displacements reach $\Delta\tilde{\nu}^{solv} = 1851\ cm^{-1}$ (cyclohexane–dichloromethane). Additionally, reduced solubility of some compounds in cyclohexane and acetonitrile causes turbidity even at 10 μM concentration.

Furthermore, all studied compounds are fluorescent in highly diluted solution in non-polar solvents. The normalized emission spectra of **N1**, **N2**, **N9**, **N15**, and **N14** in cyclohexane are depicted in Figure 8, all other spectra of TOTs and TOBs are

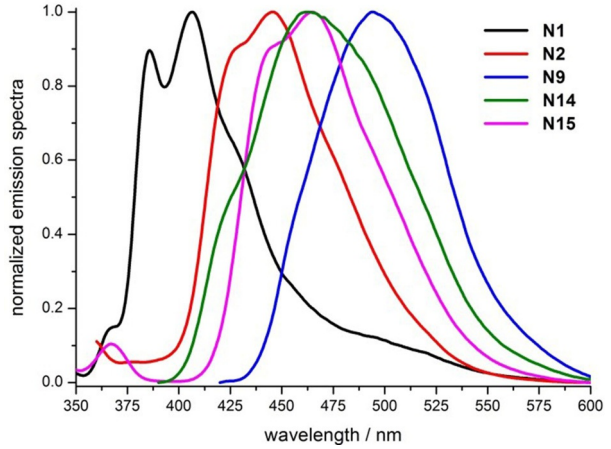

Figure 8. Emission spectra of TOTs with increasing donor substitution (**N1**, **N2**, **N9**) and increasing size of conjugated system (**N2**, **N14**, **N15**; cyclohexane).

given in the supporting information. Like excitation, the emission maxima for TOBs appear at significantly lower wavelengths than TOTs (**C3**: λ_{max}=326, λ^{fl}_{max} = 396 nm; **N2**: λ_{max}=382, λ^{fl}_{max}500 nm) and the Stokes shifts are smaller for TOBs ($\Delta\tilde{\nu}^{St}_{toluene}$(**C3**) = 5422 $< \Delta\tilde{\nu}^{St}_{toluene}$(**N2**) = 6178 cm^{-1}) (Table 5). The significant shift of excitation and emission maxima to lower energy of 1,3,5-triazine derivatives relative to the benzene analogues is due to the higher acceptor effect of the central electron-deficient triazine. Again, the polarized intramolecular charge distribution causes higher local dipole moments which are more stabilized in polar solvents. Fluorescence quantum yields were determined using quinine sulfate as reference.[43] The quantum yields of TOTs in highly diluted cyclohexane solution (approx. 0.15 μM) are moderate to high: **N1** (19%), **N2** (64%), **N9** (40%), **N15** (18), **N14** (27%) and TOBs have even higher quantum yields: **C3** (80%) and **C9** (81%).

An increasing number of alkoxy substituent (**N1** < **N2** < **N9**) enhances the donor–acceptor character that results in bathochromic shifts of emission maxima. According to the extended π-system of **N15** (biphenyl) and **N14** (naphthyl), their emission peaks appear at slightly lower energies than those of the shorter dialkoxyphenyl star **N2**.

Table 5. Optical spectroscopy.

	Solvent	λ_{max} [nm]	logε	$\lambda_{0.1}$ [nm]	λ^{fl}_{max} [nm]	$\Delta\tilde{\nu}^{St}$ [cm^{-1}]
N1	CH	380	3.39	nd	407	1746
	Tol	364	4.83	406	450	5250
	DCM	371	4.75	420	478	6034
	AN	356		406	–	
N2	CH	382	4.55	440	446	3756
	Tol	382	4.60	439	500	6178
	DCM	390	4.57	453	–	–
N3	Film	382			581	
N6	Film	382			555	
C3	CH	324	4.81	360	375	4389
	Tol	326	4.84	364	396	5422
	DCM	325	4.83	364	428	7500
	AN	337	4.58	nd	464	7792
	Film	326			409	
N9	CH	380	4.60	438	494	6073
	Tol	379	4.60	437	524	7301
	DCM	383	4.56	451	501	6150
	Film	380			565	
C9	CH	321	4.78	361	390	5772
	Tol	323	4.80	360	419	7093
	DCM	320	4.81	359	462	9466
	Film	–			450	
N14	CH	385	4.45	nd	463	4376
	Tol	394	4.50	452	503	5500
	DCM	401	4.48	478	–	–
	AN	371	4.36	nd	559	8065
N15	CH	362	4.54	nd	465	6119
	Tol	383	4.72	441	519	6842
	DCM	388	4.65	464	–	–
	AN	377	4.72	nd	559	8795

Solvents: CH: cyclohexane; Tol: toluene, DCM: dichloromethane, AN: acetonitrile, $\lambda_{0.1}$ = absorption edge at 10% of λ_{max}; nd: not determined due to turbidity.

Comparison of the emission of TOTs with similar 1,2,3-triazole derivatives reveals that the latter emit at much higher energies (λ^{fl}_{max} = 415–471 nm, THF), whereas the thiophene congener of **N9** emits with λ^{fl}_{max} = 528 nm (CH_2Cl_2).[17,18,34]

With an increasing solvent polarity, the emission maxima are shifted to lower energies, solvatochromic shifts (cyclohexane–dichloromethane) up to $\Delta\tilde{\nu}^{solv} = 3650\ cm^{-1}$ (**N1**) have been recorded. The moderate positive solvatochromism of the emission is accompanied by an efficient fluorescence quenching in polar solvents, for example, in acetonitrile and even dichloromethane. This effect correlates with the increasing donor–acceptor character.

In addition to polarity, concentration has a detrimental effect on the emissivity. THF solutions with triazine star concentrations of about 5×10^{-4} M are essentially not emissive. Dilution to 5×10^{-5} M in THF allows a weak emission which increases dramatically upon further dilution to 5×10^{-7} M. Compared with the concentrated (10^{-4} M) solutions, the fluorescence efficiencies increase by a factor of 1.4×10^{4} (**N2**) and 2.9×10^{4} (**N9**) upon dilution to 10^{-7} M. Although benzene-centered stars are less sensitive to self-quenching, dilution from 5×10^{-4} M to 5×10^{-5} M enhances the fluorescence efficiency by a factor of 45 (**C3**) or 28 (**C9**) but the emission maximum of TOBs is independent from the concentration. However, a dilut-

ed solution of **N2** emits with $\lambda^{fl}_{max}=562$ nm, 37 nm more on the red side than a concentrated solution whereas λ^{fl}_{max} of **N9** shifts to the blue, from 440 to 422 nm. For investigation of optical properties in the solid state, **N3**, **C3**, **N6**, **N9**, and **C9** with a 3,4- and 3,4,5-substitution pattern and central triazine or benzene ring were studied as representative examples. Although films of TOBs and TOTs show absorption maxima very similar to the dyes in solution, the long-wavelength tail of triazine stars brings a yellow (**N6**) or orange-red color (**N3**, **N9**). The impact of the environment on the emission is more pronounced. TOBs emit blue light whereas the emission of TOTs is yellow (**N9**: $\lambda^{fl}_{max}=567$,$\lambda^{fl}_{0.1}=642$ nm; **N3**: $\lambda^{fl}_{max}=580$ nm, $\lambda^{fl}_{0.1}=651$ nm).

A comparison of solution and film spectra reveals that the interaction of the π-systems of TOTs strongly affects the emission. Although the emission maxima of solid TOBs are blue-shifted compared with a dichloromethane solution (**C3**: $\Delta\tilde{\nu}=-1025$, **C9**: $\Delta\tilde{\nu}=-676$ cm^{-1}), the π–π interaction in solid TOTs gives rise to large bathochromic shifts. These exceed the effect of the polar dichloromethane by $\Delta\tilde{\nu}=2260$ cm^{-1} (**N9**, $\lambda^{fl}_{max}=565$ nm) or even $\Delta\tilde{\nu}=3027$ cm^{-1} (**N2/N3**, $\lambda^{fl}_{max}=580$ nm). Branching in the side chains (**N6**, 4-ethyloctyloxy) requires more space and deranges the π–π interaction, the yellow film emits with $\lambda^{fl}_{max}=554$ nm ($\lambda^{fl}_{0.1}=633$ nm). The strong intermolecular electronic interaction of excited **N9** in the solid state is in sharp contrast to the behavior of the thiophene analogue,[34] which emits at higher energies ($\Delta\tilde{\nu}=-254$ cm^{-1}) compared with a dichloromethane solution. Furthermore, the emission of films of TOTs and TOBs is temperature-dependent (Figure 9 and Supporting Information). Pristine TOT films emit with $\lambda^{fl}_{max}=581$ (**N3**), 555 (**N6**), and 570 nm (**N9**). Heating into the mesophase (150 °C) provokes significant blue-shifts ($\lambda^{fl}_{max}=536$ (**N3**), 538 (**N6**), and 531 nm (**N9**)). Upon cooling to 25 °C, these maxima loose intensity (**N3**: 15, **N6**: 15, **N6**: 23%), whereas the intensity in the long-wavelength shoulder (**N3**: $\lambda=569$, **N6**: $\lambda=565$, **N6**: $\lambda=570$ nm) is not affected. The impact of temperature on the emission of TOTs with linear side chains **N3** ($\Delta\tilde{\nu}=1941$ cm^{-1}), **N9** ($\Delta\tilde{\nu}=1288$ cm^{-1}) is higher than of **N6** ($\Delta\tilde{\nu}=569$ cm^{-1}) with branched chains. A slow reorganization process (**N6** > **N9** > **N3**) shifts the fluorescence back to longer wavelengths.

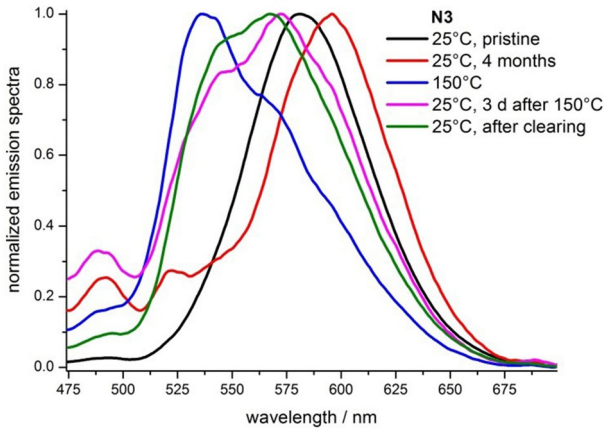

Figure 9. Emission spectra of **N3** at 150 °C and at 25 °C with different thermal history.

Unlike the TOTs, only variation of the fluorescence intensity, but no significant spectral changes occurred upon changing the temperature of films of TOBs. A film of **C3** on glass loses about 24% of its emissivity upon cooling from 150 °C to 25 °C. Surprisingly, the same experiment with **C9** gives an initial fluorescence enhancement (24%) upon cooling from 150 °C, followed by reduction of the fluorescence to 87% (at 25 °C) of the initial intensity (150 °C). Here again, in addition to the particular electronic structure, the specific molecular order in the columns controls the electronic properties.

Adding water or heptane as poor solvents to solutions of TOTs (**N2**, **N9**) and TOBs (**C3**, **C9**) in THF results in the formation of aggregates (concentration of stars in all solutions: 0.3–0.5 mM). In addition to turbidity, the effect on absorption is very individual.

Heptane (up to 90% in THF) has no significant effect on the absorption spectra of **C3**, **C9**, or **N9**, but generates a long-wavelength shoulder of **N2** at 470 nm. Water, a highly polar nonsolvent (50–90%), shifts λ_{max} to the red (≤50 nm). The more impressive part is the change of emission behavior: although the solutions in THF (0.3–0.5 mM) are essentially non emissive, the suspensions of aggregates in the mixed solvents are! Compounds **N2** ($\lambda^{fl}_{max}=507$) and **N9** ($\lambda^{fl}_{max}=517$ nm) in THF/heptane mixtures emit at lower energies than in THF/water mixtures (**N2**:$\lambda^{fl}_{max}=470$; **N9**: $\lambda^{fl}_{max}=468$ nm), but the opposite is true for the benzene analogues (**C2**:$\lambda^{fl}_{max}=390$ (heptane), $\lambda^{fl}_{max}=413$ nm (water); **C9**: $\lambda^{fl}_{max}=412$ (heptane), $\lambda^{fl}_{max}=475$ nm (water)). A comparison of the emission of aggregates and of films reveals that the aggregates of TOTs emit at significantly higher energies than TOTs in solution cast films ($\lambda^{fl}_{max}=564$–580 nm) whereas λ^{fl}_{max} of TOBs in THF/water peak at lower energies.

Clearly, the electronic spectra of these stars, especially those with a triazine center, are strongly controlled by intermolecular interactions. Surprisingly, a concentration quenching of the fluorescence in solution is opposed by aggregation-induced emission. This and the different optical properties of aggregates and films imply a plethora of molecular arrangements of triazine-centered stars.

Conclusions

Two series of discotic molecules composed of three alkoxyaryl-1,3,4-oxadiazolyl arms attached to a benzene center or electron-deficient triazine core were synthesized through threefold Huisgen reaction of tetrazoles with trimesic acid trichloride and 2,4,6-tris(chlorocarbonyl)-1,3,5-triazine as central rings. The latter is much more sensitive and requires a modified procedure. Almost all di- and tri-alkoxy substituted TOTs and TOBs exhibited thermotropic mesophases with the characteristic textures of hexagonal columnar arrangements. A variation of chain number and length allows for the control of the width of mesophase. In general, triazine derivatives have broader

mesophases ($\Delta T \leq 220$ K) than benzene analogues ($\Delta T \leq 170$ K). The mesophases are enantiotropic even though several TOTs are crystallization inhibited.

X-ray diffraction and density measurements on oriented fibers proved the dense packing of all derivatives in high temperature hexagonal columnar phases. The 3,4,5-substituted derivatives (**C9**, **N9**) stack with average π–π distances of 3.4–3.5 Å and with 18 alkyl chains in a columnar stratum of approximately 7 Å height, that is, with two molecules. Although the carbon analogue **C9** showed a strong π-stacking signal, this signal is reduced for the triazine derivative **N9**, presumably, because of electrostatic repulsion. In contrast, the two chain derivatives **C2** and **N2** contain three molecules in a columnar recurrence between 7.5–7.7 Å. Again, the number of chains sum up to 18, but three aromatic cores fill now the center of the columns, in which a coplanar stacking is not possible anymore. For all derivatives, a denser packing can be achieved with a Y-shaped conformer of the star, minimizing the intrinsic free space.[44]

The charge carrier mobilities of TOBs and TOTs ($\mu = 10^{-3}$–10^{-5} $cm^2 V^{-1} s^{-1}$) are in the medium range of discotic liquid crystals.

TOBs are colorless and TOTs are yellow to red substances, their emission behavior is largely controlled by intermolecular interactions. Efficient emission in highly diluted solution, concentration quenching, aggregation-induced emission (enhancement), modulation of fluorescence by solvent polarity, temperature, and aggregation are optical phenomena that complement the thermal mesomorphism.

Experimental Section

Synthetic procedures, analyses, spectra, and equipment are collected in the Supporting Information

Acknowledgements

The authors gratefully acknowledge Dr. Johannes Liermann (NMR), Prof. Dr. F. Laquai (ToF), M. Müller (DSC) and Dr. C. Kampf (MS), Dr. D. Schollmeyer (Single Crystal X-ray Scattering), the Deutsche Forschungsgemeinschaft (DE 515/9-1) for partial funding and the Carl-Zeiss Stiftung for a generous fellowship (N.T.).

Conflict of interest

The authors declare no conflict of interest.

Keywords: fluorescence · heterocycles · liquid crystals · solvatochromism · X-ray scattering

[1] B. Roy, N. De, K. C. Majumdar, *Chem. Eur. J.* **2012**, *18*, 14560 – 14588.
[2] S. Laschat, A. Baro, N. Steinke, F. Giesselmann, C. Hägele, G. Scalia, R. Judele, E. Kapatsina, S. Sauer, A. Schreivogel, M. Tosoni, *Angew. Chem. Int. Ed.* **2007**, *46*, 4832 – 4887; *Angew. Chem.* **2007**, *119*, 4916 – 4973.
[3] U. H. F. Bunz, J. Freudenberg, *Acc. Chem. Res.* **2019**, *52*, 1575 – 1587.
[4] S. Kumar, *Chemistry of Discotic Liquid Crystals: From Monomers to Polymers*, CRC, Boca Raton, **2011**.
[5] V. Balzani, G. Bergamini, P. Ceroni, *Angew. Chem. Int. Ed.* **2015**, *54*, 11320 – 11337; *Angew. Chem.* **2015**, *127*, 11474 – 11492.
[6] a) L. Schmidt-Mende, *Science* **2001**, *293*, 1119 – 1122; b) C. W. Tang, *Appl. Phys. Lett.* **1986**, *48*, 183; c) I. Seguy, P. Jolinat, P. Destruel, J. Farenc, R. Mamy, H. Bock, J. Ip, T. P. Nguyen, *J. Appl. Phys.* **2001**, *89*, 5442.
[7] a) W. Pisula, A. Menon, M. Stepputat, I. Lieberwirth, U. Kolb, A. Tracz, H. Sirringhaus, T. Pakula, K. Müllen, *Adv. Mater.* **2005**, *17*, 684 – 689; b) T. Hassheider, S. A. Benning, M. W. Lauhof, R. Oesterhaus, S. Alibert-Fouet, H. Bock, J. W. Goodby, M. D. Watson, K. Muellen, H.-S. Kitzerow, in *Liquid Crystal Materials, Devices, and Applications IX* (Ed.: L.-C. Chien), SPIE, Bellingham, **2003**, pp. 167 – 174.
[8] D. Adam, P. Schuhmacher, J. Simmerer, L. Häußling, W. Paulus, K. Siemensmeyer, K.-H. Etzbach, H. Ringsdorf, D. Haarer, *Adv. Mater.* **1995**, *7*, 276 – 280.
[9] B. R. Kaafarani, *Chem. Mater.* **2011**, *23*, 378 – 396.
[10] M. Bäker, *Funktionswerkstoffe*,; Springer, Wiesbaden, **2014**.
[11] a) D. Demus, J. W. Goodby, G. W. Gray, H. W. Spiess, V. Vill, *Handbook of Liquid Crystals*; Wiley-VCH, Weinheim, **2011**; b) T. Wöhrle, I. Wurzbach, J. Kirres, A. Kostidou, N. Kapernaum, J. Litterscheidt, J. C. Haenle, P. Staffeld, A. Baro, F. Giesselmann, S. Laschat, *Chem. Rev.* **2016**, *116*, 1139 – 1241.
[12] a) S.-H. Wu, H.-H. Chen, *Tetrahedron* **2019**, *75*, 220 – 229; b) N. Röder, T. Marszalek, D. Limbach, W. Pisula, H. Detert, *ChemPhysChem* **2019**, *20*, 463 – 469; c) C. Cuerva, J. A. Campo, P. Ovejero, M. R. Torres, E. Oliveira, S. M. Santos, C. Lodeiro, M. Cano, *J. Mater. Chem. C* **2014**, *2*, 9167 – 9181.
[13] a) S. Kumar, *Chem. Soc. Rev.* **2006**, *35*, 83 – 109; b) H. Detert, M. Lehmann, H. Meier, *Materials* **2010**, *3*, 3218 – 3330.
[14] a) M. Talarico, R. Termine, E. M. García-Frutos, A. Omenat, J. L. Serrano, B. Gómez-Lor, A. Golemme, *Chem. Mater.* **2008**, *20*, 6589 – 6591; b) M. Vadivel, I. S. Kumar, K. Swamynathan, V. A. Raghunathan, S. Kumar, *ChemistrySelect* **2018**, *3*, 8763 – 8769; c) A. Gowda, L. Jacob, D. P. Singh, R. Douali, S. Kumar, *ChemistrySelect* **2018**, *3*, 6551 – 6560.
[15] a) J. Luo, B. Zhao, J. Shao, K. A. Lim, H. S. O. Chan, C. Chi, *J. Mater. Chem.* **2009**, *19*, 8327; b) H. Taing, J. G. Rothera, J. F. Binder, C. L. B. Macdonald, S. H. Eichhorn, *Liq. Cryst.* **2018**, *45*, 1147 – 1154; c) K.-C. Zhao, J.-Q. Du, H.-F. Wang, K.-Q. Zhao, P. Hu, B.-Q. Wang, H. Monobe, B. Heinrich, B. Donnio, *Chem. Asian J.* **2019**, *14*, 462 – 470; d) D. Tian, Y. Zhou, Z. Li, S. Liu, J. Shao, X. Yang, J. Shao, W. Huang, B. Zhao, *ChemistrySelect* **2017**, *2*, 8137 – 8145; e) L. Zhang, D. L. Hughes, A. N. Cammidge, *J. Org. Chem.* **2012**, *77*, 4288 – 4297.
[16] a) J. Han, *J. Mater. Chem. C* **2013**, *1*, 7779; b) E. Beltrán, J. L. Serrano, T. Sierra, R. Giménez, *Org. Lett.* **2010**, *12*, 1404 – 1407.
[17] a) E. Beltrán, J. L. Serrano, T. Sierra, R. Giménez, *J. Mater. Chem.* **2012**, *22*, 7797 – 7805; b) B. Feringán, P. Romero, J. L. Serrano, R. Giménez, T. Sierra, *Chem. Eur. J.* **2015**, *21*, 8859 – 8866.
[18] a) H. Meier, M. Lehmann, H. C. Holst, D. Schwoeppe, *Tetrahedron* **2004**, *60*, 6881 – 6888; b) A. Navarro, M. P. Fernández-Liencres, G. García, J. M. Granadino-Roldán, M. Fernández-Gómez, *Phys. Chem. Chem. Phys.* **2015**, *17*, 605 – 618.
[19] K. Naito, A. Miura, *J. Phys. Chem.* **1993**, *97*, 6240 – 6248.
[20] S. Varghese, N. S. S. Kumar, A. Krishna, D. S. S. Rao, S. K. Prasad, S. Das, *Adv. Funct. Mater.* **2009**, *19*, 2064 – 2073.
[21] Y.-D. Zhang, K. G. Jespersen, M. Kempe, J. A. Kornfield, S. Barlow, B. Kippelen, S. R. Marder, *Langmuir* **2003**, *19*, 6534 – 6536.
[22] a) T. Curtius, F. H. Dellschaft, *J. Prakt. Chem.* **1901**, *64*, 419 – 438; b) R. Stollé, H. P. Stevens, *J. Prakt. Chem.* **1904**, *69*, 366 – 381; c) B. Pradhan, S. K. Pathak, R. K. Gupta, M. Gupta, S. K. Pal, A. S. Achalkumar, *J. Mater. Chem. C* **2016**, *4*, 6117 – 6130; d) K. Kotwica, A. S. Kostyuchenko, P. Data, T. Marszalek, L. Skorka, T. Jaroch, S. Kacka, M. Zagorska, R. Nowakowski, A. P. Monkman, A. S. Fisyuk, W. Pisula, A. Pron, *Chem. Eur. J.* **2016**, *22*, 11795 – 11806.
[23] S. K. Pathak, R. K. Gupta, S. Nath, D. S. S. Rao, S. K. Prasad, A. S. Achalkumar, *J. Mater. Chem. C* **2015**, *3*, 2940 – 2952.
[24] a) R. Huisgen, J. Sauer, H. J. Sturm, J. H. Markgraf, *Chem. Ber.* **1960**, *93*, 2106 – 2124; b) D. D. Prabhu, N. S. S. Kumar, A. P. Sivadas, S. Varghese, S. Das, *J. Phys. Chem. B* **2012**, *116*, 13071 – 13080.
[25] E. Girotto, J. Eccher, A. A. Vieira, I. H. Bechtold, H. Gallardo, *Tetrahedron* **2014**, *70*, 3355 – 3360.
[26] a) H. Detert, E. Sugiono, G. Kruse, *J. Phys. Org. Chem.* **2002**, *15*, 638 – 641; b) H. Detert, *Synthesis* **1999**, 999 – 1004.

[27] S. H. Gihm, B. G. Kim, S. Kim, J. Seo, S. Y. Park, C. R. Park, *J. Mol. Struct.* **2010**, *984*, 371 – 375.
[28] G. Xu, L. Zheng, S. Wang, Q. Dang, X. Bai, *Synth. Commun.* **2010**, *40*, 361 – 369.
[29] R. Cristiano, D. M. Pereira de Oliveira Santos, H. Gallardo, *Liq. Cryst.* **2005**, *32*, 7 – 14.
[30] T. Rieth, S. Glang, D. Borchmann, H. Detert, *Mol. Cryst. Liq. Cryst.* **2015**, *610*, 89 – 99.
[31] A.-A. S. El-Ahl, S. S. Elmorsy, A. H. Elbeheery, F. A. Amer, *Tetrahedron Lett.* **1997**, *38*, 1257 – 1260.
[32] T. Rieth, T. Marszalek, W. Pisula, H. Detert, *Chem. Eur. J.* **2014**, *20*, 5000 – 5006.
[33] R. Cristiano, H. Gallardo, A. J. Bortoluzzi, I. H. Bechtold, C. E. M. Campos, R. L. Longo, *Chem. Commun.* **2008**, 5134 – 5136.
[34] T. Yasuda, T. Shimizu, F. Liu, G. Ungar, T. Kato, *J. Am. Chem. Soc.* **2011**, *133*, 13437 – 13444.
[35] CCDC 1894806 (**N1**) contain the supplementary crystallographic data for this paper. These data are provided free of charge by The Cambridge Crystallographic Data Centre.
[36] A. R. Katritzky, S. K. Singh, N. K. Meher, J. Doskocz, K. Suzuki, R. Jiang, G. L. Sommen, D. A. Ciaramitaro, P. J. Steel, *ARKIVOC* **2006**, 43 – 62.
[37] K. Navamani, K. Senthilkumar, *J. Phys. Chem. C* **2014**, *118*, 27754 – 27762.
[38] H. Muraoka, M. Mori, S. Ogawa, *Phosphorus Sulfur Silicon Relat. Elem.* **2015**, *190*, 1382 – 1391.
[39] P. Scherrer, *Nachr. Ges. Wiss. Goettingen* **1918**, *2*, 98 – 100.
[40] B. Donnio, B. Heinrich, H. Allouchi, J. Kain, S. Diele, D. Guillon, D. W. Bruce, *J. Am. Chem. Soc.* **2004**, *126*, 15258 – 15268.
[41] A. Immirzi, B. Perini, *Acta Crystallogr. Sect. A* **1977**, *33*, 216 – 218.
[42] V. Lemaur, D. A. da Silva Filho, V. Coropceanu, M. Lehmann, Y. Geerts, J. Piris, M. G. Debije, A. M. van de Craats, K. Senthilkumar, L. D. A. Siebbeles, J. M. Warman, J.-L. Brédas, J. Cornil, *J. Am. Chem. Soc.* **2004**, *126*, 3271 – 3279.
[43] J. R. Lakowicz, *Principles of Fluorescence Spectroscopy*, Springer, New York, **2010**.
[44] M. Lehmann, M. Dechant, M. Lambov, T. Ghosh, *Acc. Chem. Res.* **2019**, *52*, 1653 – 1664.

Manuscript received: June 28, 2019
Accepted manuscript online: August 19, 2019
Version of record online: November 4, 2019

